

The ENSO Signal in the Northwest Pacific

Vladimir Ponomarev, Olga Trusenkova, Serge Trousenkov,
Dmitry Kaplunenko, Elena Ustinova, and Antonina Polyakova
Pacific Oceanological Institute Russian Academy of Sciences
pacific@online.marine.su

Abstract

The oscillations of the El Niño–Southern Oscillation (ENSO) scale (3–7 years) in oceanographic and meteorological characteristics in the Northwest Pacific are studied. Monthly mean sea surface temperature (SST) for the period of 1947–1978 was subjected to the Complex Empirical Orthogonal Functions (CEOF) analysis in time domain to study moving features in SST anomaly patterns in the North Pacific. Both unlagged and lagged correlations were found between air temperature at the Northwest Pacific Margin coastal meteorological stations for the 20th century or ice extent in the Sea of Okhotsk for the second part of the 20th century with SOI. Meteorological situations were also considered over the North Pacific based on the classification developed by Polyakova (1992, 1997). Six principal types of synoptic situations represented by characteristic sea level pressure (SLP) fields are associated mainly with different locations of cyclone tracks and of high/low pressure over the North Pacific. It was shown that the ENSO signal with a lag of about half a year may be associated with the Northwest Pacific Ocean memory in a seasonal cycle. The ENSO signal with a lag of about one year is probably conditioned by both oceanic SST anomalies propagating from the tropic–equatorial Pacific to the extratropic areas and by the atmosphere circulation response to these anomalies.

1. Introduction

The El-Niño - Southern Oscillation (ENSO) is an oscillation of a 3–7 year period in the atmosphere–ocean system (Bjerknes, 1969) observed mainly in the equatorial/tropical Pacific as an alternation of El Niño/La Niña events in the ocean (Wyrtki, 1975) and Southern Oscillation in the atmosphere studied by numerous researchers started from the pioneer work of Walker (1924).

El Niño, or warm phase of ENSO, is an oceanographic phenomenon of warm surface water pool formation offshore of the coasts of Ecuador and Peru, accompanied by the following events:

- Subtropic High Pressure weakens in the Southeast Pacific while sea level pressure (SLP) rises over Australia–Indonesian area that corresponds to negative phase of Southern Oscillation (negative values of Southern Oscillation Index – SOI);
- typical Walker circulation and southern/northern hemisphere trade winds weaken;
- atmospheric convection area of Walker circulation shifts eastward from the western (Australia–Indonesian area) to the central tropical/equatorial Pacific and South America maritime area;
- westerly winds originate over the area of the western and central equatorial Pacific;
- a warm sea surface temperature (SST) anomaly moves east to the central eastern equatorial Pacific while a cold anomaly forms in the western area;
- heating decreases in the western tropical Pacific and South Asian winter monsoon weakens;
- meridional winds and Hadley circulation weaken in the western area and shift eastward;
- low winter and spring rainfall in the Australia–Indonesian area with Australian summer monsoon onset late and generally poor.

The modern state of the problem is described as achievements of the TOGA Program (*Learning to Predict Climate Variations Associated with El Niño and Southern Oscillation, Accomplishments and Legacies of the TOGA Program*, 1996) where most of the important recent scientific results related to ENSO, including the extratropic response to ENSO and its relationship with the Asian–Australian monsoon (Yang and Webster, 1990), are also outlined.

To explain the reason and physical mechanism of ENSO, the basic idea of coupled atmosphere–ocean instability in tropics was suggested in early 80s (Philander et al., 1984). The unstable coupled atmosphere–ocean mode was found using shallow water atmosphere–ocean models (Philander et al., 1984; Hirst, 1986).

At the same time, a lot of meteorological and oceanographic data, observed in both the tropics and extratropics during ENSO events were collected and analyzed particularly on the basis of the TOGA project. As suggested, irregularity of ENSO may be caused by nonlinearity in the ocean–atmosphere system and interactions between ENSO and anomalies of the annual cycle in the tropics and extratropics. Substantial anomalies of ENSO cycles and changes of El Niño and La Niña occurrences during winters from 1950 to 1995 were shown by Zhang and Wallace (1996) and many others. In particular, La Niña occurrences in winter have dramatically decreased since 1977. After a maximum interval between El Niño events from 1974 to 1982, La Niña events have become weaker and have taken place mostly in summer while El Niño has dominated in winter and has become more frequent since 1987.

According to Sekine and Yamada (1996) and Sekine (1998), the ENSO cycle has a feedback from anomalies of winter snow coverage over the Asian continent and summer monsoon winds. In this case, the large-scale processes in the mid-latitude impact on ENSO.

Therefore, the main goal of our study is to find new evidence of ENSO accompanying events in the mid-latitude Northwest Pacific on the basis of meteorological and oceanographic data analyses.

The present work contains:

- a brief background review of the tropic–extratropic relationship associated with ENSO;
- an interpretation of SST anomaly development and movement in the North Pacific using the Complex Empirical Orthogonal Functions (CEOF) method;

- an estimation of the statistical relationship between ENSO and anomalies of meteorological/ oceanographic characteristics in the Northwest Pacific Margin;
- a discussion of typical synoptic situations, their variations, and impact on the subarctic West Pacific Margin.

In the following review earlier studies on the extratropic response to ENSO are discussed which are related to, or promote better understanding of, our findings.

2. Background on the tropic-extratropic relationship associated with ENSO

The extratropic response to ENSO is mostly considered as a global scale phenomenon in the coupled ocean–atmosphere system. It is explained by the ENSO impact on hemispheric patterns of geopotential height and upper ocean temperature anomalies (Bjerknes, 1969; Horel and Wallace, 1981; Trenberth and Paolino, 1981; Alexander, 1992a,b; Lau and Nath, 1990; Palmer, 1993; Molteni et al., 1993).

The part of the variance associated with long-term variability of different scales reaches its maximal values in the subarctic zonal belt. Therefore, the extratropic response to ENSO in the atmosphere seems to be obscured and highly nonlinear (Geisler et al., 1985) due to its interaction with internally generated oscillations. In turn, the internally generated mid-latitude SST variations may overwhelm the signal from anomalies of tropical heating (Trenberth, 1995).

Palmer (1993) and Molteni et al. (1993) argued that, despite very large natural variability of the extratropical circulation, there exist certain preferred regimes with rather persistent flow patterns presumably associated with the land–sea distribution and climatological planetary waves. The effect of tropical SST forcing alters the frequency of occurrence and stability of certain pre-existing regimes (*Learning to Predict Climate Variations Associated with El Niño and Southern Oscillation. Accomplishments and Legacies of the TOGA Program*, 1996).

The principal questions related to our study are as follows: what kinds of large-scale circulation processes in the North Pacific atmosphere influence the extratropical regimes and, at the same time, are the most closely related to the tropic–extratropic interaction and to ENSO. Those are known to be the meridional Hadley circulation, westerly jet stream and

monsoon circulation. Effects of heating displacement in the tropics on the location and intensity of Hadley circulation and westerly jet stream (Lau and Boyle, 1987; Yang and Webster, 1990; Hou, 1993; Oort and Yienger, 1996), as well as on the monsoon system anomalies (Tanaka, 1982; Schucla and Paolino, 1983; Wu and Hastenrath, 1986; Webster and Yang, 1992; Webster et al., 1997) are actually considered as important physical devices of the extratropic response to ENSO in the atmosphere.

Physical processes of synoptic scale which actualize the ENSO-scale remote linkages in the atmosphere are actually associated with propagation of faster, barotropic (Simmons et al., 1983) and slower, baroclinic (Blackmon et al., 1977; Lau and Boyle 1987; Hou, 1993) waves as well as with changes of extratropical storm tracks (Branstator, 1995) and tropical cyclone activity in the Western Pacific (Chan, 1985; Chen and Weng, 1998).

As for oceanic teleconnections, the poleward ENSO signal propagation in the North Pacific Ocean was described by Johnson and O'Brien (1990a,b). Based on circulation model and observation data analysis they showed that temperature and upper layer thickness anomalies propagate northward along the eastern coast of North America due to coastal Kelvin waves and reach the 50°N latitude in about one year. Westward temperature anomaly propagation to the central Pacific is due to baroclinic Rossby waves excited by coastal Kelvin waves.

Thus, one can suggest that, at least in the North Pacific, both a northward fast ENSO signal in the atmosphere and slow ENSO signal in the ocean exist. Propagation of both these signals is controlled by synoptic-scale processes, atmospheric ones of order of a week, and oceanic ones of order of a few months, which, in turn, interact with larger-scale processes. An oceanic signal propagating northward along the eastern Pacific boundary and westward offshore to the subtropical central Pacific more pronounced while an atmospheric signal is rather obscured in the extratropic area.

It seems that the atmospheric ENSO signal may be dominant in the Northwest Pacific Margin due to its interaction with the Asian monsoon system in southern (tropic-subtropic) and northern (subarctic) areas. This suggestion is supported by previous studies on data analyses in the area of the North Asian monsoon and westerly jet stream.

In this study we examined the relationship at zero or half-year (seasonal) lags between SOI, air tem-

perature in the Northwest Pacific Margin from the southern Japanese Kushu Island and Korean Peninsula (30°N) to the Chukchy Peninsula (70°N), and ice extent in the Sea of Okhotsk. At the same time, we analyzed ENSO (including 1997–98 El Niño–La Nina events) accompanying meteorological situations over the extratropic North Pacific and how their occurrence is related to seasonal/monthly air temperature and ice extent anomalies. To estimate the oceanic response to ENSO in the Northwest Pacific Margin we also analyzed propagation of winter SST anomalies using complex EOF method.

3. Data and Methods

To estimate the propagation of SST anomalies in the North Pacific, the archive of monthly mean SST was used. It consists of 384 time counts for 32 years from 1947–1978 taken in 163 5° × 5° grid points for the area of 20–55°N, 120°E–120°W. A time period was chosen up to 1978 so that the recent shift in climate regime occurred in 1976 which resulted in changes of occurrence of El Niño–La Niña events is not included in the consideration. It is a subject of further analysis to estimate an impact of this change upon anomaly patterns in the North Pacific.

To study moving features in the anomaly patterns, the complex principal components analysis in time domain was applied to signals composed of original SST data. Theoretical development of the method can be found in Brillinger (1975) and Horel (1984). Conventional (unfiltered) anomalies were computed by subtracting temperature mean values for every month, thus removing the climatic seasonal cycle. Asymmetric filtering (Enting and Robbins, 1989) was applied to obtain signals representing variability in different time scales (Section 4).

Time series of monthly mean air temperature at meteorological stations in the Northwest Pacific Margin for the 20th century, mainly up to 1990, and 10-day mean ice extent for the Okhotsk and Bering Seas from 1960 to 1998 (Plotnikov, 1997) were chosen for estimation of seasonal links with ENSO by correlation analysis (Section 5).

To consider atmosphere conditions over the North Pacific associated with ENSO and their impact on the Northwest Pacific Margin, time series (days/month) of frequency of occurrence were analyzed for six synoptic situations as SLP fields over the mid-latitude North Pacific from 1949 to 1998 based on the classification and calendar developed by Polyakova (1992, 1997). Correlation analysis

was used to reveal their relationship with ENSO based upon both lagged and unlagged correlation estimates (Section 6).

4. Interpretation of SST Anomaly Development and Movement in the North Pacific

The decomposition of ocean/atmosphere fields into normal spatial and temporal components known as an empirical orthogonal function (EOF) analysis is widely applied to reconstruct anomaly patterns in space. Filtering, harmonic and spectral analyses are performed to study variability in time. However, standard EOF analysis is not able to separate moving oscillations from standing ones or directly estimate anomaly propagation. For this reason, an alternative method of complex empirical orthogonal function (CEOF) for detecting moving features is currently employed when eigenvalues and eigenvectors are computed for cross spectrum matrix (frequency domain method; Brillinger, 1975) or complex covariance matrix (time domain method; Horel, 1984). In the latter case, complex signals are first composed of initial scalar fields when an imaginary part is taken as the Gilbert transform of a real part (original data). CEOFs and time series of complex principal components (PCs) obtained are characterized by amplitude and phase (hereafter referred to as spatial/temporal amplitude and phase); power spectra of PC time series are calculated to estimate time-scales of variability.

Movement of monthly mean SST anomalies in the mid-latitude central North Pacific area for the period of 1947–1976 was earlier estimated by Michaelsen (1982) applying CEOF analysis in frequency domain. He showed that SST anomalies propagate in the northeastward direction in a dominant frequency band of about 0.02 cpm (cycles per month; inverse months). The corresponding period of 4.2 years can be associated with the characteristic ENSO period.

Trousnev (1991) applied CEOF techniques in time domain for SST anomalies in the North Pacific (20°–55°N, 120°E–120°W) based on the archive of monthly mean SST described in Section 3. Figure 1 shows (a) spatial amplitude and (b) phase for the first CEOF (20% of variance). A high amplitude belt spreads in the tropical region and eastern and central Pacific areas, with maximum amplitudes located near the North American coast from 35°N to 45°N. According to the spatial phase, anomalies

associated with the first CEOF propagate along the axis between the northeastward and southeastward corners of the basin, tending to bypass the Northwest Pacific area where spatial amplitude is minimal.

The power spectrum of the first PC covers a wide range of time scales from 5 months to 10 years but has an absolute maximum ENSO time scale (3.5–5.3 years). It also has weaker 1.5- and 1-year peaks and intra-annual peaks with periods of 7–8 and 5–6 months (Figure 2a). Lagged correlation coefficients were calculated between the first PC temporal amplitude and SOI/Nino3 Index (Figure 3a). Correlation curves of the PC amplitude with SOI and Nino3 are symmetrical along the x -axis which is obviously due to high negative correlation between the SOI and El Niño Index, so it is enough to use either one for further analysis.

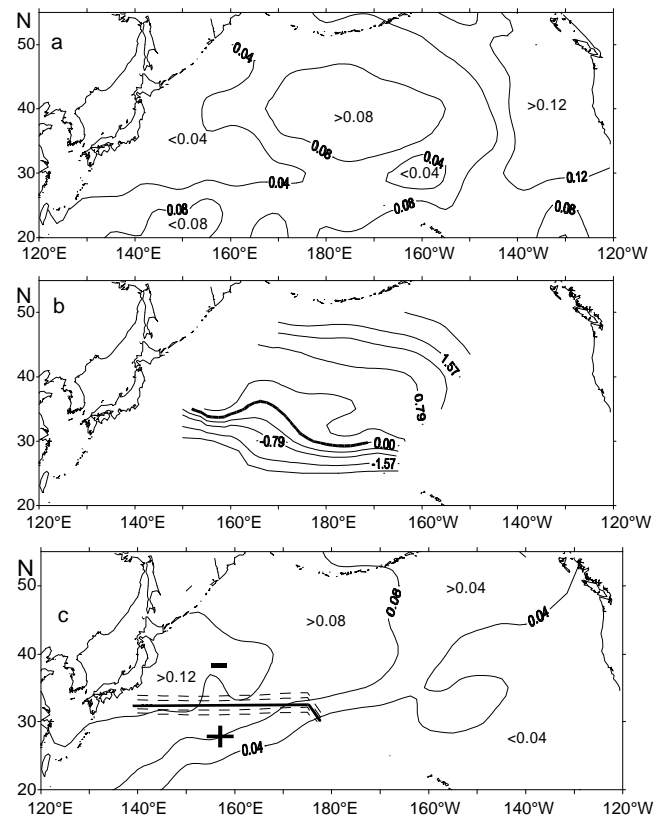


Figure 1. (a) Spatial amplitude and (b) phase of the first CEOF and (c) spatial amplitude and phase of the second CEOF for the unfiltered monthly SST anomalies in the extra-tropical North Pacific (1947–1978). Phase is given in radians. For the second CEOF, zero phase contour is shown as a thick solid line and phase contours of $-p$, $-p/2$, $p/2$, p are shown as dashed lines, with signs indicating areas of positive (+) and negative (–) phases.

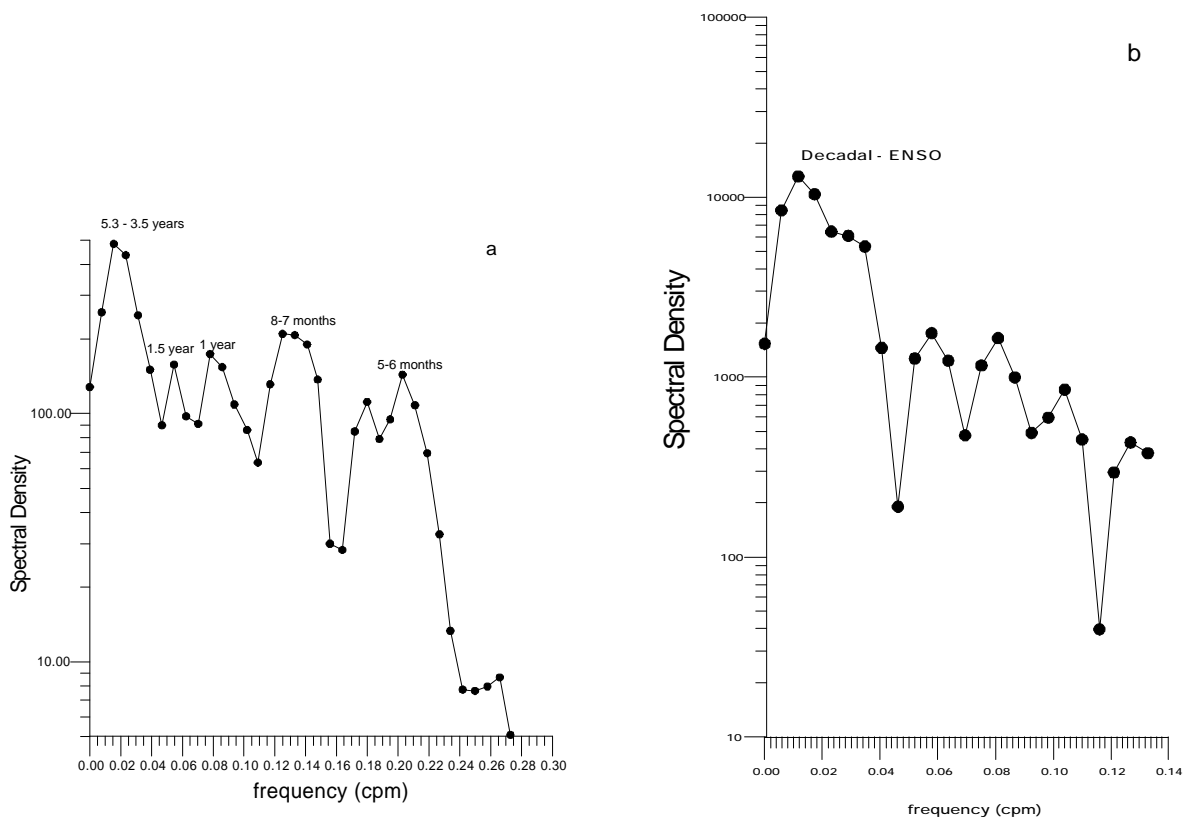


Figure 2. Power spectra of (a) the first temporal PC for the unfiltered monthly SST anomalies and (b) the second temporal PC for low-pass pre-filtered monthly mean SST in the extra-tropical North Pacific (1947–1978).

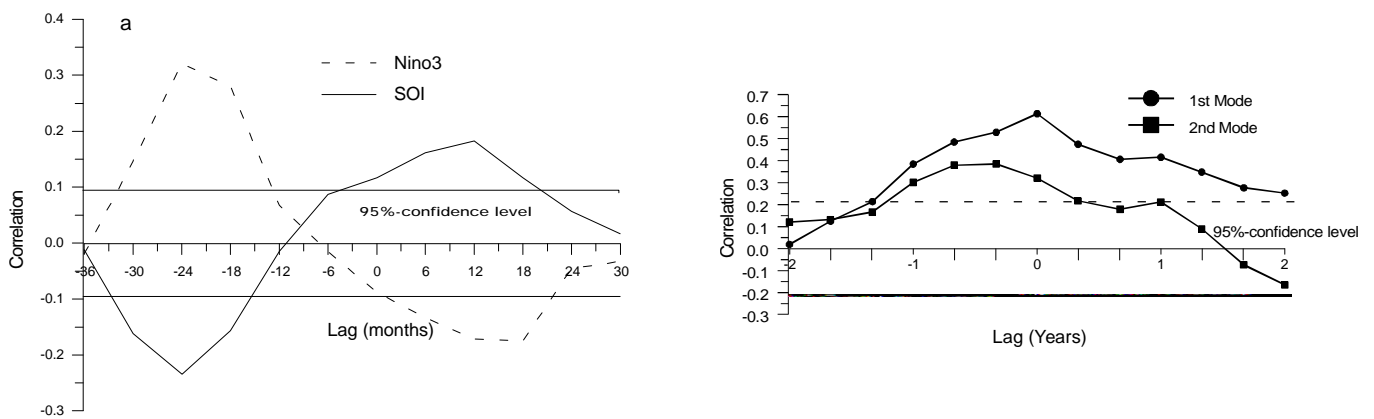


Figure 3. Lagged correlation of (a) the first temporal PC for the unfiltered monthly SST anomalies with SOI and Niño3 Index and (b) the first and second temporal PCs for the low-pass pre-filtered winter SST anomalies with the low-pass pre-filtered El Niño Index in the extra-tropical North Pacific (1947–1978).

Substantial asynchronous links with 1.5–1 year (–18, –24 months in the x -axis, Figure 3a) SST anomaly delay were obtained as well as weaker but statistically significant links with 1 year (+12 months in the x -axis, Figure 3a) SOI/Niño3 Index delay. Asynchronous links obtained are characteristic for the entire North Pacific where the first CEOF spatial amplitude is high with the exception of the Northwest Pacific where the spatial amplitude is low (Figure 1a). Periodicity of the correlation coefficient as a function of lag is about 5 years which corresponds to the ENSO time scale. Positive lagged correlation with SST anomalies behind Niño3 corresponds to positive anomalies over the extra-tropic North Pacific as a whole formed in 1.5–2 years after the El Niño event. This is consistent with general idea of oceanic ENSO teleconnection (Johnson and O’Brien, 1990a,b, and many others). Negative lagged correlation with Niño3 behind SST anomalies points out that ENSO seems to have a positive feedback with extra-tropic North Pacific SST anomalies.

However, the first PC temporal phase (not shown) implies that SST anomalies can propagate in either direction along the northeast–southwest axis as phase mostly decreases with time but increases in some periods. (When the temporal phase gradually increases/decreases, a wave propagates from lower/higher to higher/lower values of spatial phase; abrupt phase jumps are due to its being conventionally bounded in a range from $-\pi$ to π .) This can be explained by the fact that analyzed time series consist of anomalies of varied time scales. So, pre-filtered narrow-band data should be processed to obtain patterns for SST anomalies of a certain time scale.

On the contrary, the second CEOF of unfiltered SST anomalies (12% of variance) shows the standing wave with the amplitude localized in the western Pacific with maximum amplitude in the area of 35° – 45° N (Figure 1c). The western subarctic area is in anti-phase with the western subtropical area, the dividing line is stretched along 32 – 33° N, in the area of the Kuroshio Extension. The contour line of zero phase is also shown in the Figure 1c as a thick solid line and dashed lines represent phases of $-\pi$, $-\pi/2$, $\pi/2$, π . (Abrupt rise and fall of phase on both sides of the zero contour means that the second CEOF is a standing oscillation.)

To separate time scales further analysis was performed based upon filtered time series both of SST and their anomalies.

To estimate contribution of a seasonal signal into propagation of temperature waves in the North Pacific seasonal SST time series were obtained by applying a band-pass filter with a band of 0.05–0.1 cpm (corresponding periods of 9–21 months) to the original SST fields. The CEOF method in time domain was applied to the filtered SST. The general (first) seasonal CEOF (93% of variance) is a standing wave in the subtropical Pacific where the western area is in phase with the eastern one and they both are in the anti-phase with the central area. No moving features were found for the seasonal signal, so, this pattern may be explained by sea–land contrasts and atmosphere–ocean interaction in a annual cycle.

To remove short-time (seasonal and bi-annual) signals from the monthly SST time series a low-pass filter with periods longer than 21 months was applied to the original monthly SST. In this case, with the absence of intra-annual and bi-annual variations in the signal, the general (first) mode (97% of variance) shows no oscillate features and it does not have significant local maxima in its spectrum. The second CEOF (1% of variance) has high amplitudes, mainly in the western subarctic Pacific (the area to the north of 40° N adjacent to Hokkaido and Kuril Islands) as shown in Figure 4a. The spatial phase pattern (Figure 4b) shows that this mode is a superposition of a progressive and standing waves. As for

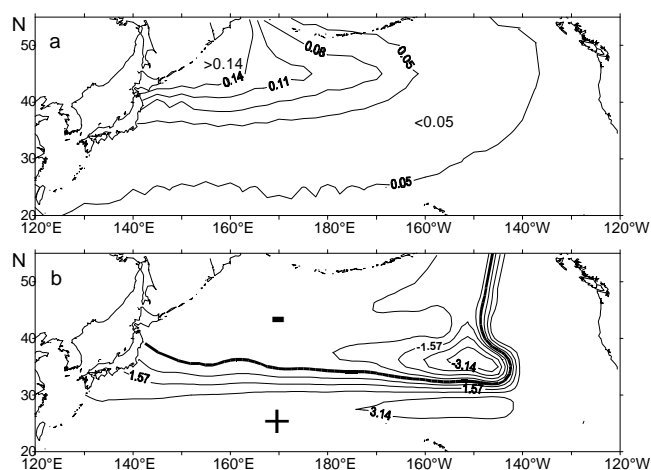


Figure 4. (a) Spatial amplitude and (b) phase of the second CEOF for the low-pass pre-filtered monthly mean SST in the extra-tropical North Pacific (1947–1978). Phase is given in radians. Contour line of zero phase is shown as a thick solid line.

the standing oscillation, its pattern is similar to the second mode for conventional SST anomalies but with a sharper outlined area of maximum amplitudes. However, the second PC temporal spectrum has high values in a range of 4.8–10 years with maximum at 7.2 years (Figure 2b).

Thus, analysis for pre-filtered SST time series shows that there are no progressive waves left in general CEOFs for either seasonal or interannual signals. It is concluded that propagating features should be associated with SST anomalies rather than SSTs themselves. Lack of progressive oscillations in the two general modes of low-pass filtered SST component covering 98% of total variance is evidence that moving disturbances are associated with SST anomalies the in seasonal cycle. This gave grounds to believe that winter anomalies would be more informative.

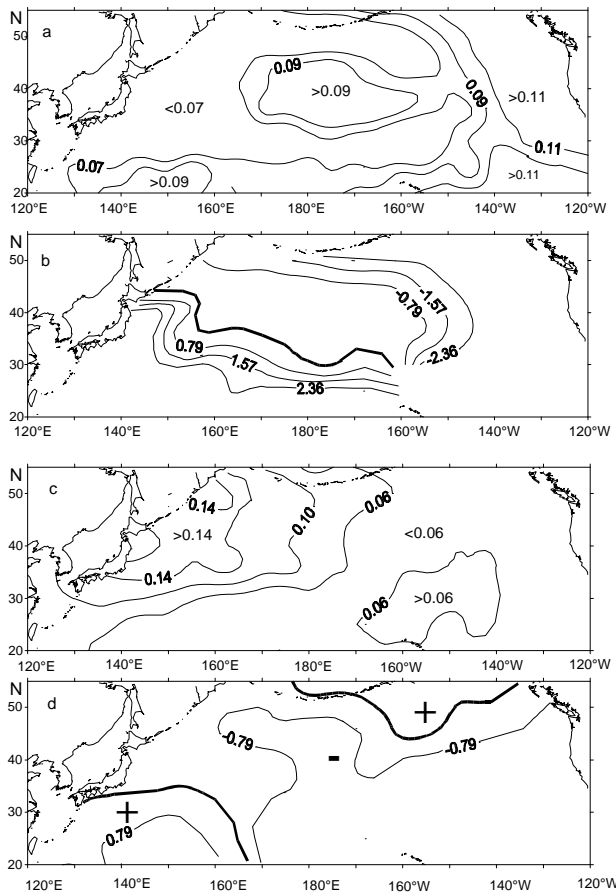


Figure 5. (a) Spatial amplitude and (b) phase of the first CEOF and (c) spatial amplitude and (d) phase of the second CEOF for the low-pass pre-filtered winter SST anomalies in the extra-tropical North Pacific (1947–1978). Phase is given in radians. Zero phase contour is shown as a thick solid line. Signs indicate areas of positive (+) and negative (–) phases.

The same low-pass filtering and CEOF procedures were applied to SST monthly anomalies taken for winters only. Time series consist of SST anomalies taken for December, January and February of every year (96 time counts). A maximum of spatial amplitude for the first CEOF (29% of variance) corresponds to the known Kelvin wave propagating along the eastern Pacific coast. Another spatial amplitude maximum corresponds to the Rossby wave propagating in the westward direction from the eastern coast to the central midlatitude Pacific area (Figure 5a) confirmed by the spatial (Figure 5b) and temporal (not shown) phases. Spatial phase gradients suggest that SST anomalies propagate westward from the eastern Pacific margin up to 155–160°W in the belt of 30–40°N (Figure 5b), in line with the Johnson - O’Brien model (Johnson and O’Brien, 1990a, b).

Anomaly wave turns southwestward from the spatial amplitude maximum area (30–40°N, 170°E–160°W). Significant spatial phase gradients and, therefore, southwestward wave propagation are characteristic of the entire western subtropic Pacific. It corresponds to the results of ocean surface level data analysis (ERS 1 satellite three-day repeat altimeter data) on southwestward propagation of waves in the area of 30–40°N, 145–160°E off the Japanese coast (Minster and Gennero 1995).

The first PC temporal amplitude for low-pass pre-filtered winter SST anomalies seems to be correlated to the monthly low-pass pre-filtered El-Niño Index time series taken for winters only. Its lagged correlation (Figure 3b) is positive and statistically significant within –1 year (PC amplitude delayed) and +2 year (PC amplitude leading) lag range. It reaches its maximum of 0.61 at a zero lag, i.e. for unlagged correlation. Unlike lagged links of the first PC for unfiltered SST anomalies (Figure 3a), high synchronic correlation of the first PC for low-pass filtered winter SST anomalies with the El Niño Index points out to the possible impact of ENSO-accompanying processes in the winter extratropical atmosphere. The spectrum of the first PC (Figure 6a) has its absolute maximum shifted to decadal time-scales (“red shift”) compared to the spectrum for unfiltered SST anomalies (Figure 2a).

Unlike the first CEOF, the second mode for pre-filtered winter SST anomalies (16% of variance) shows maximum amplitudes in the western Pacific in the belt of 30°–55°N (Figure 5c). Spatial (Figure 5d) and temporal (not shown) phases reveal the signal propagating from the central Pacific (45°N,

175°E–175°W) in the opposite directions: southwestward in the western subtropic area and northeastward in the eastern subarctic area. This is similar to the finding of Mizuno and White (1983) based on analysis of 300-m temperature data (from 1976–1980, at 30°–40°N, 130°–180°E) that in the Kuroshio Extension area temperature waves propagate westward in the area to the west of the Shatsky Rise (155°E) and eastward to the east of there.

The second PC temporal amplitude also shows a correlation with the pre-filtered winter El Niño Index although lower in value compared to the first mode (Figure 3b). However, in this case, correlation is statistically significant for zero lag and delays up to 1 year only. The spectrum of the second PC (Figure 6b) has its absolute maximum in a wider range including decadal and ENSO scales, compared to the spectrum for unfiltered SST anomalies (Figure 2a). Thus, removing short-scale variations from SST anomalies reveals decadal together with ENSO variations both in the first and second modes.

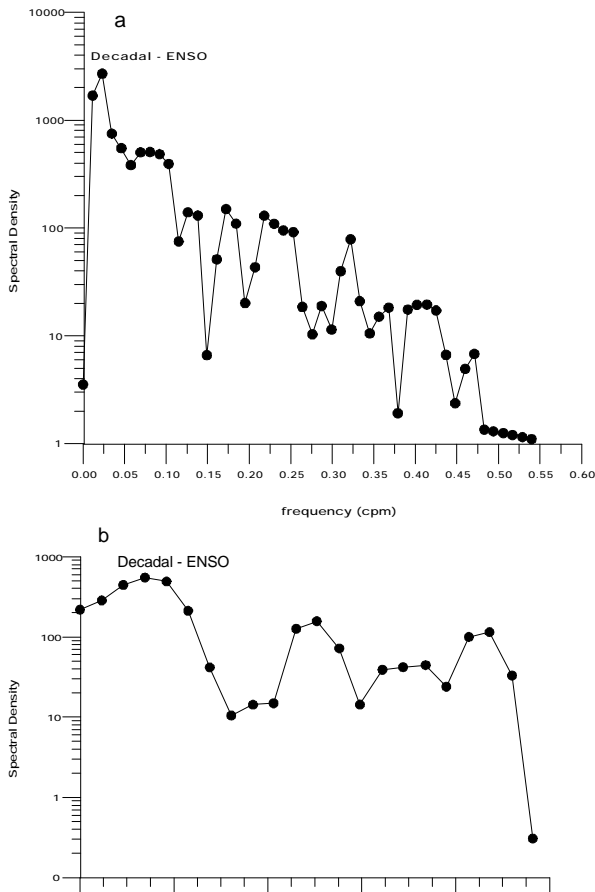


Figure 6. Power spectra of (a) the first and (b) the second temporal PCs for the low-pass pre-filtered winter SST anomalies in the extra-tropical North Pacific (1947–1978).

Recently, a substantial interest has arisen to studies on decadal variation which are considered generated in midlatitudes. Analyzing SST anomalies along the coast of the Sea of Japan for the period from 1930/40 to 1984, Watanabe et al. (1986) showed that while 6-year variations dominate in an area adjacent to the Korean Strait, the decadal scale prevails in the northwestern area. Nakamura et al. (1997) applied EOF (not complex) analysis to winter mean SST anomalies for the North Pacific to analyze decadal variations removing ENSO and lower-scale signals. Spatial patterns obtained by Nakamura et al. for the first and second EOFs are similar to our second and first CEOF spatial amplitudes obtained for the pre-filtered winter SST anomalies, correspondingly (Figure 5c,a); namely, the mentioned pairs show common areas of high amplitude. However, compared to Nakamura et al.'s first EOF, in our case, an area of high amplitude for the second CEOF is shifted to the west to the transition area between Oyashio–Kuroshio Current Systems where the most intensive ocean–atmosphere interaction takes place in winter. The presence of both decadal and ENSO variations in SST as well as synchronic correlation of PCs with SOI gives evidence of feedback between decadal and ENSO time-scale dynamic processes in the ocean–atmosphere system in this area which is consistent with findings of Sekine and Yamada (1996) and Sekine (1998).

5. Seasonal Links between ENSO and Air Temperature in the Northwest Pacific Margin

Characteristic time scales of infra-annual air temperature variations in the Northwest Pacific Margin were obtained from power spectra for stations located in the area from the Korean to Chukchy Peninsulas. Spectra were estimated based on monthly mean time series for the 20th century, often more than 100 years, taken separately for every month. We chose the three following intervals of interest in the time-scale: biennial (2–3 years), quasi-ENSO (3–7 years), and quasi-decadal (7–13 years) intervals.

As a typical example, periods obtained for stations located around the Japan Sea are shown in the Table 1. It includes all spectral maximums of 95%-significance level and shows that every chosen time interval has, as a rule, the only maximum. Well known biennial variations are present at all stations for almost all months. ENSO and decadal scale variations are also present at almost all stations for

1–2 months at least. Decadal variations become more pronounced at the continental stations, on the one hand, and at the subarctic stations, on the other hand. In particular, one can see from the Table 1 that along the Japanese Islands coast decadal variations are present in winter at the Akita and Supporo

stations located to the north of 39°N. As for the Nikolaevsk station located to the north of Tatar Strait at the Okhotsk Sea coast, decadal variations are present for 7 months of a year. This is typical for most stations around the Sea of Okhotsk, the including Kamchatka Peninsula coast.

Table 1. Characteristic time scales of monthly mean air temperature variations for Russian, Korean and Japanese meteorological stations around the Japan Sea taken from spectra calculated for every monthly time series separately. 95% confidence level is accepted. Underlined are values corresponding to the middle of ENSO (3.0–6.9) or decadal (7.0–12.9) periods.

Month	Station	Time scale			Station	Time scale		
		2.0–2.9 (biennial)	3.0–6.9 (ENSO)	7.0–12.9 (decadal)		2.0–2.9 (biennial)	3.0–6.9 (ENSO)	7.0–12.9 (decadal)
1	Nikolaevsk (53°9'N, 140°4'E) 1925–1990 (66 years)	2.1		7.3	Sapporo (45°N, 141°14'E) 1889–1990 (102 years)	2.2		7.8
2		2.1		12.8		2.0	<u>4.4</u>	12.8
3			<u>4.1</u>				<u>4.1</u>	<u>11.3</u>
4		2.6		<u>11.0</u>		2.6		<u>11.3</u>
5		2.3	<u>5.1</u>			2.6	<u>4.6</u>	
6		2.6				2.0	<u>5.4</u>	
7			<u>6.0</u>			2.2	3.0	
8		2.0		<u>11.0</u>		2.9	<u>6.0</u>	
9		2.0				2.4	<u>6.4</u>	
10		2.4		<u>11.0</u>		2.6		<u>11.3</u>
11		2.4		<u>11.0</u>		2.3	<u>4.6</u>	
12				<u>9.4</u>		2.1	3.6	<u>8.5</u>
1	Vladivostok (43°7'N, 131°5'E) 1881–1990 (110 years)	2.2			Akita (39°26'N, 140°5'E) 1886–1990 (105 years)	2.2		8.0
2			<u>4.2</u>			2.0	<u>4.5</u>	<u>11.6</u>
3		2.1	<u>3.9</u>				<u>4.0</u>	<u>11.6</u>
4		2.0		7.3		2.6		
5		2.0	3.3	7.9		2.0	<u>4.7</u>	
6		2.0	3.0			2.3	<u>5.2</u>	
7			3.0			2.9	<u>5.2</u>	
8			<u>5.8</u>				<u>6.5</u>	
9		2.2	3.4			2.2	<u>5.8</u>	
10		2.3	<u>4.2</u>			2.5		
11		2.3;	3.1			2.4	<u>4.3</u>	
12		2.2		<u>9.2</u>		2.4	3.6	<u>9.5</u>
1	Mokpho (34°53'N, 126°33'E) 1905–1990 (86 years)	2.2		7.8	Fukuoka (33°21'N, 130°15'E) 1890–1990 (101 years)	2.3	3.7	
2			<u>3.9</u>			2.2	<u>5.9</u>	
3		2.3	<u>6.6</u>				<u>4.0</u>	
4		2.2		<u>8.6</u>			3.0	
5			<u>4.5</u>				<u>4.0</u>	
6		2.2	3.2			2.0		
7			3.1			2.0	3.0; <u>5.9</u>	
8			6.6			2.9		
9		2.8		7.2		2.8;	6.7	
10		2.6	<u>5.7</u>			2.6		
11		2.4	<u>5.7</u>			2.2	<u>4.3</u>	
12		2.3		<u>9.6</u>		2.3	3.1	

1	Inchon	2.3	<u>4.8</u>		Nagasaki	2.2	3.6	
2	(37°27'N,	2.3	<u>5.7</u>		(32°45'N,	2.2	3.6	<u>9.3</u>
3	126°37'E)		<u>3.9</u>	<u>9.6</u>	129°50'E)		<u>4.0</u>	
4		2.9		<u>8.6</u>		2.2	3.0	
5		2.9		<u>10.8</u>		2.9		
6	1905–1990	2.3			1879–1990	2.1		
7	(86 years)		<u>5.1</u>		(112 years)	2.0	<u>5.6</u>	
8			<u>5.4</u>				3.0	
9		2.0		7.2		2.7		
10		2.6	<u>6.0</u>			2.6		
11		2.3	<u>5.4</u>			2.2	<u>6.2</u>	
12		2.5		<u>8.6</u>		2.3	3.1	<u>10.0</u>

Table 2. Correlation matrix for time series (1940–1990) of the winter mean air temperature at coastal meteorological stations around the Sea of Okhotsk with each other and Southern Oscillation Index averaged for the same winter (SOI), next summer (SOI, +6) and previous summer (SOI, -6). Only statistically significant correlation is shown (95%-confidence level).

	Okhotsk	Ajan	Icha	Nikolaevsk	Alexndrvsk	Poronaysk	Abashiry	Nemuro	SOI	SOI, +6 m.	SOI, -6 m.
Magadan	0.93	0.53	0.79	0.42	0.43	0.52	none	none	0.54	none	0.43
Okhotsk		0.66	0.71	0.58	0.52	0.59	none	none	0.58	none	0.38
Ajan			0.48	0.68	0.78	0.69	0.4	0.47	0.41	none	none
Icha				0.46	0.57	0.59	0.46	0.47	0.51	none	0.42
Nikolaevsk					0.73	0.66	0.5	0.52	0.38	none	0.32
Alexndrvsk						0.84	0.71	0.75	0.42	none	0.28
Poronaysk							0.49	0.57	0.56	none	0.43
Abashiry								0.97	none	none	none
Nemuro									none	none	none

Spectra for time series (about 100 years) of winter 3- and 5-month (December–February and November–March) mean air temperature for meteorological stations located around the Japan Sea and SOI are shown in Figure 7. Air temperature spectra exhibit only two maximums, one corresponding to biennial variations and the other maximum shifted to the decadal scale (7–9 years). Figure 7 also shows that spectral density significantly increases from the southeast to the northwest. Spectra estimated for the Okhotsk Sea and Pacific coasts of the Kamchatka Peninsula show similar patterns. This is consistent with the spectrum for the second PC of low-pass filtered winter SST anomalies which has a wide maximum in a range of decadal and ENSO scales (Figure 6b) while the area of maximum spatial amplitudes of this CEOF covers the western subarctic Pacific. As for air temperature time series averaged for summer, spring or fall for stations located around the southern Japan Sea, the dominating maximum corresponds, as a rule, to the typical ENSO time-scale.

Thus, the presence of well pronounced ENSO and decadal scale variations in the subarctic area corresponds to findings based on the analysis of North Pacific winter SST (Nakamura et al., 1997, results of the present study) as well as of Oyashio Intrusion and snow coverage over the eastern Asia (Sekine and Yamada, 1996). Therefore, the relationship between seasonal air temperature anomalies with ENSO should be analyzed.

To reveal seasonal links between SOI and air temperature in the Northwest Pacific correlation analysis was applied. Lagged and unlagged correlation coefficients were calculated between time series of SOI and air temperature averaged for 5 (November–March or May–September) and 3 months (December–February or June–August) at the meteorological stations in the Northwest Pacific Margin. Lagged correlation was estimated between air temperature time series taken for winter and SOI taken for the previous (time lag of -6 months) or next summer (time lag of 6 months). Examples of correlation coefficients calculated for the period of 1940–

1990 are shown in Table 2.

Statistically significant unlagged positive correlation between winter mean air temperature and SOI was found for stations located at the Sakhalin, Siberian and Kamchatka coasts of the Okhotsk Sea. It means that air temperature tends to have a positive anomaly during winter La Niña events and a negative anomaly during winter El Niño events. An example for air temperature at the Ust-Hairuzovo meteorological station located at the Kamchatka coast of the Okhotsk Sea superimposed with North Pacific Index (NPI) and SOI is shown in Figure 8. The correlation coefficient with SOI is statistically significant with a 95%-confidence level and equal to 0.55.

Moreover, total ice coverage in the Okhotsk Sea also shows a linear relationship with SOI (Figure 9). A 10-day mean time series (1957–1989) was calculated by averaging the ice extent during periods of greater ice cover for every year (21–28 of

February, 1–10, 11–20 and 21–30 of March, and 1–10 of April). Its unlagged correlation coefficient with SOI is equal to -0.45 with a 95%-confidence level. Its lagged correlation coefficient with SOI for a previous summer (SOI taken 6 months behind) is equal to -0.46 with a 95%-confidence level. Thus, ice coverage increases in years of winter El Niño events or in winters after summer El Niño events and decreases in years of winter La Niña events or in winters after summer La Niña events (Figure 9). (SOI has the highest negative values during El Niño events and highest positive values during La Niña events.)

At the same time, air temperature at the meteorological stations situated at the northeast Hokkaido coast (Nemuro and Abashiry) and at the south Kuril Islands, do not have a statistically significant unlagged correlation with the internal Okhotsk/Japan Sea coastal stations or SOI.

There is no lagged correlation between winter air temperature at the Okhotsk Sea coastal stations and SOI of a next summer (+6 months) while the lagged correlation between the mentioned time series and SOI of a previous summer (–6 months) is statistically significant but still smaller compared with the unlagged ones (Table 2). This is in accordance with the presence of synchronic and delayed correlation between the El Niño Index and the second temporal PC for the pre-filtered winter SST anomalies (Figure 3b) while the corresponding spatial CEOF has high amplitudes in the western subarctic Pacific (Figure 5c).

The seasonal mean air temperature time series in the meteorological stations located at the oceanic coast of Kamchatka and adjacent Komandorsky Islands also show statistically significant unlagged correlation with SOI for winter. However, no statistically significant unlagged correlation was found for air temperature and SOI at the Chukchy coast of the Bering Sea, or at the Chukchy coast of the Chukchy Sea.

As for the unlagged correlation between winter (3- or 5-month mean) air temperature at the Japan Sea coastal stations and SOI, the statistically significant coefficients were obtained mainly for the stations situated along the subarctic Northwest Japan Sea coast (Vladivostok, Nakhodka, Terney, Cape Zolotoi, Aleksandrovsk). On the contrary, 5-month summer (May–September) mean air temperature time series show a high unlagged correlation with SOI at the southern stations located along the southeastern coast of the Japan Sea (Akita,

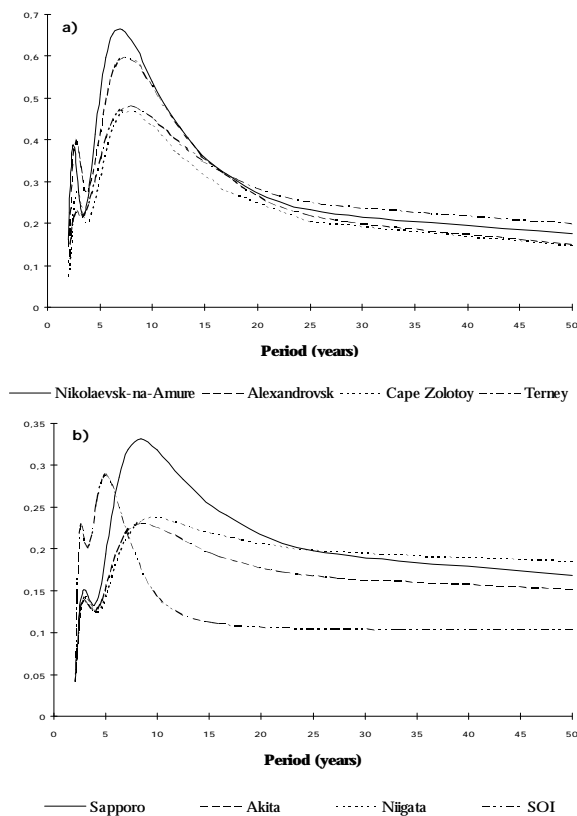


Figure 7. Power spectra for time series of SOI and winter mean (December–February) air temperature for meteorological stations located around the Japan Sea: at (a) the Siberian coast (Terney, Cape Zolotoy, Nikolaevsk-Na-Amure) and Sakhalin Island (Alexandrovsk) and at (b) the Japanese Islands (Sapporo, Akita, Niigata) and SOI.

Adgihara, Fukuoka). The significant correlation between 3-month summer (June–August) air temperature and SOI is revealed only for the most southern stations, for example Fukuoka.

So, a significant local maximum of the ENSO time scale in the spectrum of monthly mean air temperature was found for most meteorological stations

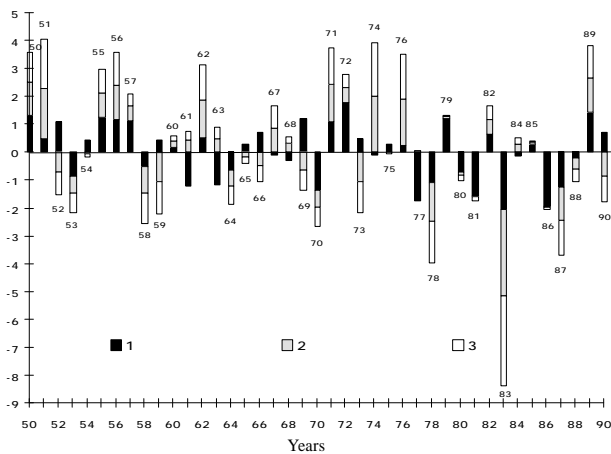


Figure 8. Time series (1950–1990) of normalized winter anomaly of (1) NPI, (2) SOI, and (3) air temperature at the Ust-Hairuzovo meteorological station located at the Okhotsk coast of Kamchatka Peninsula. (SOI positive anomalies correspond to La Niña event, negative anomalies correspond to El Niño event).

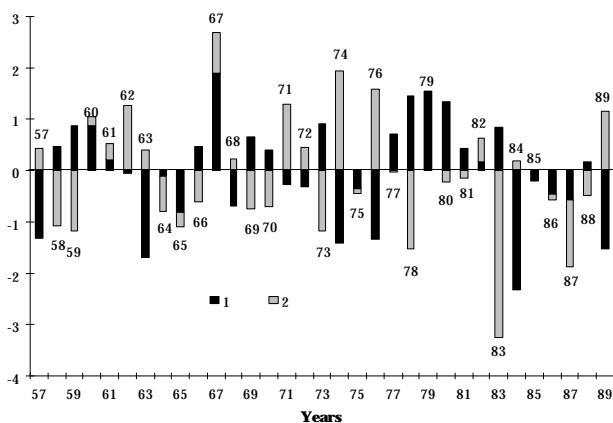


Figure 9. Time series (1957–1989) of the Sea of Okhotsk ice extent (1) normalized anomaly and (2) normalized winter anomaly of SOI. (SOI positive anomalies correspond to the La Niña event, negative anomalies correspond to the El Niño event).

in the Northwest Pacific Margin, but air temperature and SOI are related in a different way in the southern (South Japan Sea coast and Korean Peninsula), mid (Okhotsk Sea coast and Kamchatka Peninsula) and northern (Bering Sea coast and Chukchy Peninsula) areas. This difference is associated with asymmetry of the seasonal temperature anomalies in an annual cycle. Air temperature over the South Japan Sea is more under influence of ENSO-accompanying dynamic processes in the extratropical summer atmosphere, whereas air temperature over the North Japan Sea, Okhotsk Sea and Kamchatka Peninsula is mostly subjected to the impact of the ENSO accompanying processes in the winter atmosphere.

NPI measuring intensity of the Aleutian Low also has a statistically significant unlagged correlation with SOI for winter (Figure 8) but not for summer. Correlation coefficients for 5- and 3-month winter mean time series are equal to 0.58 and 0.41, respectively. Besides, lagged correlation coefficients between winter NPI and SOI taken for a previous summer (–6 months lag) are statistically significant as well and equal to 0.49 and 0.45, for 3- and 5-month averaging, respectively. At the same time, the NPI spectrum has a well known decadal spectral maximum, which is also present in the time series of air temperature (Table 1) over the Western Subarctic Pacific Margin. Ice extent in the Sea of Okhotsk shows a decadal maximum in the spectrum as well (Plotnikov, 1997).

According to air temperature and SST analyses one can suggest that ENSO and decadal scale variations in the North Pacific are connected via both annual–biennial oscillations of the Asian Monsoon and ocean–atmosphere interaction in the western mid-latitude (subarctic/subtropic) and central subtropical Pacific.

6. Typical Synoptic Situations, their Variations, and Impact on the Subarctic Northwest Pacific Margin

Polyakova (1992, 1997) developed the heuristic classification based on daily sea surface pressure (SLP) fields and suggested six principal types of atmosphere synoptic circulation over the North Pacific (Figures 10–15). The choice of original observations rather than averaged, for example monthly data, gave classes which keep information on synoptic processes.

Positions of cyclone tracks as well as of the Aleutian Low Pressure and Subtropic High Pressure Centers were chosen as classifying attributes for atmospheric circulation patterns. Characteristic synoptic situations (classes) presented as six SLP fields correspond to known atmospheric circulation patterns over the North Pacific area obtained earlier by (Wallace and Gutzler, 1981) and over the Northern Hemisphere (Barnston and Livezey, 1987) using EOF analysis of averaged SLP fields. In particular, Polyakova's expert situations reflect the Pacific–North American (PNA), East–West (EW), Zonal Dipole (ZD) patterns. The latter is similar to the Pacific Transition (PT) pattern in the hemispheric classification (Barnston and Livezey, 1987).

It was shown earlier that due to ENSO events over the Northern Hemisphere "...changes in the extratropical circulation immediately begin to change the jet stream and the associated storm tracks, so that the heat and vorticity fluxes caused by the transient eddies in the extratropics are also altered." (Branstator, 1995; citation from *Learning to Predict Climate Variations Associated with El Nino and the Southern Oscillation*, 1996). This gives grounds to believe that Polyakova's calendar of six atmosphere circulation pattern occurrences may be closely connected with ENSO accompanying events in the mid-latitude Northwest Pacific.

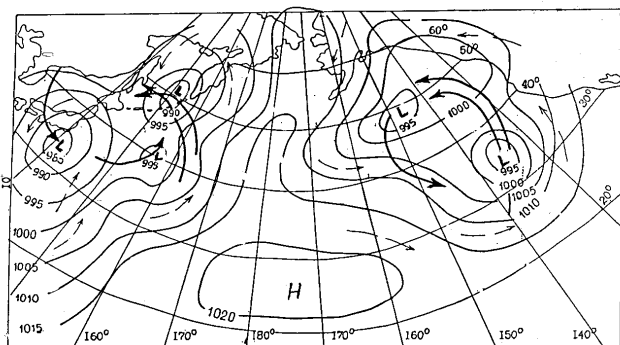


Figure 10. The Okhotsk–Aleutian (OA) synoptic situation associated with northwestward cyclone tracks in the Okhotsk Sea adjacent to the Pacific and north-eastward tracks near North America as well as with the central position of Subtropic High Pressure, strongly meridional type in the Eastern and Western Pacific. Air mass transport is shown by thin arrows, cyclone tracks are shown by thick arrows.

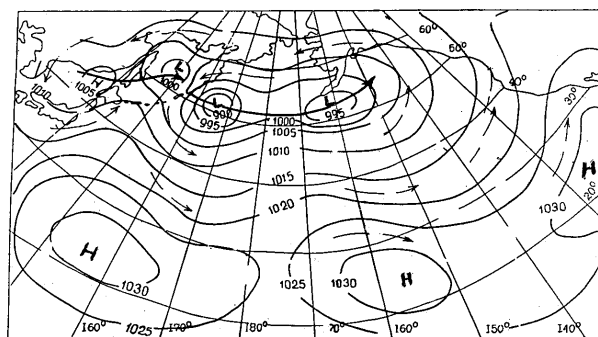


Figure 11. The Aleutian-Zonal (AZ) synoptic situation associated with zonal cyclone tracks in Subarctic Pacific (50° – 55° N) from the Sea of Okhotsk to the North America as well as with both zonally stretched Aleutian Low and Subtropic High Pressure. Air mass transport is shown by thin arrows, cyclone tracks are shown by thick arrows.

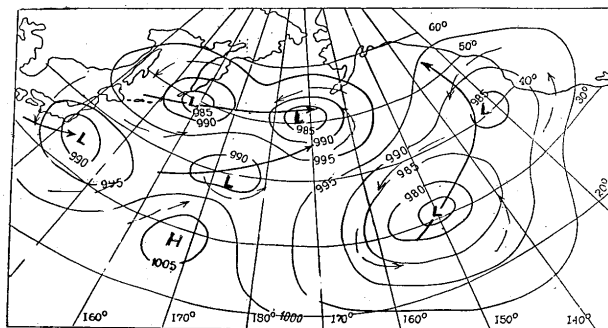


Figure 12. The Cyclones Over the North Pacific (CN) synoptic situation associated with cyclonic activity over mid-latitude (subtropic and subarctic) North Pacific, with western position of the Subtropic High Pressure and with eastward cyclone tracks in the western and central Pacific and northward tracks in the eastern Pacific. Air mass transport is shown by thin arrows, cyclone tracks are shown by thick arrows.

Three situations show a more or less pronounced meridional (Figures 10, 12, 14) and three situations show quasi-zonal (Figures 11, 13, 15) circulation patterns over the North Pacific. The former ones are associated with sea–land temperature contrasts, while the latter ones may be considered as related to south–north temperature contrasts. Higher frequency of occurrence of zonal or meridional types may accompany weakening or strengthening of both

the Asian winter and summer monsoons in the Northwest Pacific Margin, respectively. It is especially true for the subarctic Northwest Pacific area where the highest variance of both air temperature and SST anomalies of a seasonal cycle was found. A characteristic example for low-frequency variations in the subarctic Northwest Pacific is also the South Oyashio Intrusion (Hanawa, 1995; Sekine, 1996).

Thus, the classification used in the present study can be a basis for the estimation of interannual variations in both the Asian Monsoon and circulation patterns in the North Pacific atmosphere via anomalies of synoptic situation frequency of occurrence and cyclone track changes in transitions from one situation to another. Time series were composed of monthly frequency of occurrence (days per month) for these situations taken from 1949 to 1997 and averaged for 3- (December–February, June–August) and 5-month (November–March, May–September) winter or summer periods. To estimate the linear relationship with ENSO, time series of SOI were subjected to the same kind of averaging. It should be noted that the years 1990 and 1992 are missing from the Polyakova’s calendar. This was taken into account when the SOI time series were composed. The occurrence of the six synoptic situations is shown in Figure 16. It is easy to see that the first four types occur more often than the last two ones.

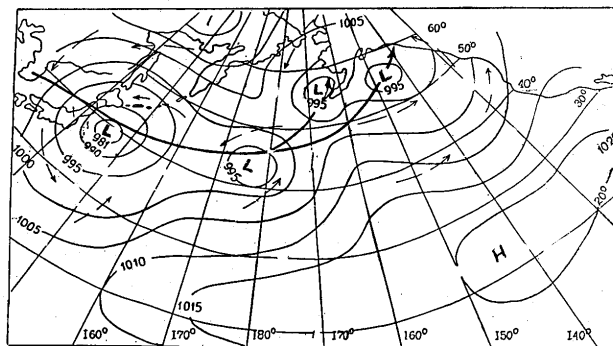


Figure 13. The Northwest (NW) synoptic situation associated with cyclonic activity over the western Subtropic and eastern Subarctic Pacific with cyclone tracks in northeastern direction and with eastern position of Subtropical High Pressure. Air mass transport is shown by thin arrows, cyclone tracks are shown by thick arrows.

The first two types, especially the Okhotsk–Aleutian (OA) situation, meridional for the whole North Pacific, correspond to the penetration of south cyclones with characteristic weather patterns into the northern Japan and southern Okhotsk Seas and Kuril area of the Pacific. On the other hand, the internal Okhotsk Sea is subjected to cold air mass transport from Siberia in winter. This sharpens the land–sea contrast and strengthens the winter monsoon. The OA situation (Figure 10) represents the classical meridional dipoles with a high pressure ridge over the central Pacific from the subtropic to subarctic area and low pressure over the eastern and

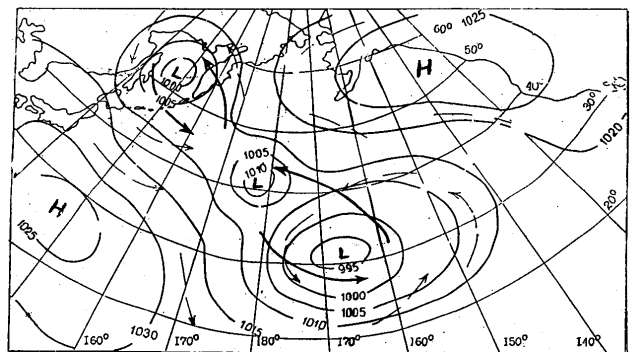


Figure 14. The Okhotsk–Hawaii (OH) synoptic situation associated with unusual cyclone tracks over the Central Pacific and Sea of Okhotsk as well as the high pressure over North America and extreme western position of the Subtropical High Pressure. Air mass transport is shown by thin arrows, cyclone tracks are shown by thick arrows.

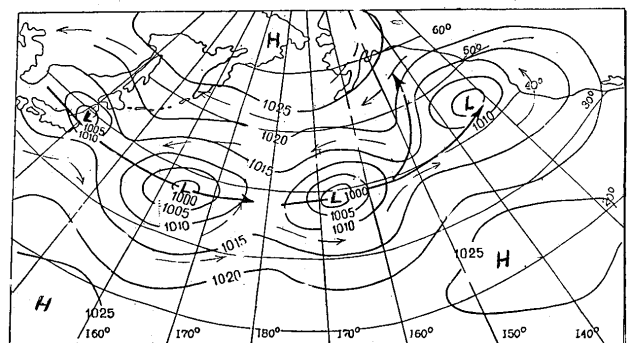


Figure 15. The Southern–Zonal (SZ) synoptic situation associated with strong zonal eastward cyclone tracks in the Western Central Pacific (35°–49°N) and northward tracks in the Eastern Pacific. Air mass transport is shown by thin arrows, cyclone tracks are shown by thick arrows.

western Pacific. Due to its high frequency of occurrence it is often present in the monthly mean fields. Northward tracks of south cyclones dominate over the western and eastern Pacific Ocean. For the western Pacific, cyclones come from the Philippine Sea through the Kuroshio–Oyashio area to the Kuril Pacific area, northern Japan and southern Okhotsk Seas.

The Aleutian-Zonal (AZ) situation (Figure 11) corresponds to a zonal dipole with low pressure in the subarctic and high pressure in the subtropic Pacific representing a pattern of an active winter monsoon. Northeastward cyclones move mostly along the land–sea margin from the East China Sea through the Japan Sea to the southern Okhotsk Sea and then turn eastward to cross the subarctic Pacific. Time series for the AZ situation winter mean frequency of occurrence shows both unlagged and lagged (6 months ahead) negative correlation with SOI. Correlation coefficients satisfy to a 95%-confidence level and are equal to -0.047 and -0.44 , respectively, which means that the AZ situation is more frequent during winter El Niño events.

The Cyclones Over the North Pacific (CN) synoptic situation (Figure 12) reveals a meridional circulation pattern in the eastern Pacific with a western position of the weakened Subtropic High Pressure, northward cyclone tracks over the Eastern Pacific, and eastward tracks over the Western Pacific.

The Northwest (NW) synoptic situation (Figure 13) exhibits an almost zonal circulation dipole pattern but still has asymmetric features. It is characterized by the southeastern position of Subtropic High with eastward cyclone tracks over the Kuroshio–Oyashio Extension area in the western Pacific and northeastward tracks over the eastern subarctic Pacific. Both the CN and NW situations have a similar effect on the Okhotsk Sea due to cyclone tracks located over the southern Sea. The NW situation frequency of occurrence shows a positive unlagged correlation with SOI of 0.37 , slightly above the 95%-confidence level. It means that the NW situation is less frequent during winter El Niño events.

Two last synoptic situations (Figures 14 and 15) are very rare events compared to the previous ones (Figure 16). The Okhotsk–Hawaii (OH) situation represents a kind of exotic feature of the atmosphere circulation over the North Pacific. It exhibits a diagonal dipole similar to an extreme phase of PNA with low pressure over the subarctic and central Pacific and high pressure over North America.

The latter prevents northward propagation of the cyclone in the eastern Pacific area. Subtropical High Pressure is located in an extreme southwestern position blocking the northward cyclone tracks in this area. There are rather cold (subarctic) cyclones above the Okhotsk Sea in winter.

The Southern-Zonal (SZ) situation (Figure 15) corresponds to a zonal dipole with an extreme southern position of the subarctic low pressure system, high pressure over the Bering Sea and Alaska, eastward cyclone tracks in the subtropic Pacific area and northeastward cyclone tracks over subarctic eastern Pacific. Both these situations cause cold winter air temperature anomalies in North America, but their impact on the Northwest Pacific is not significant.

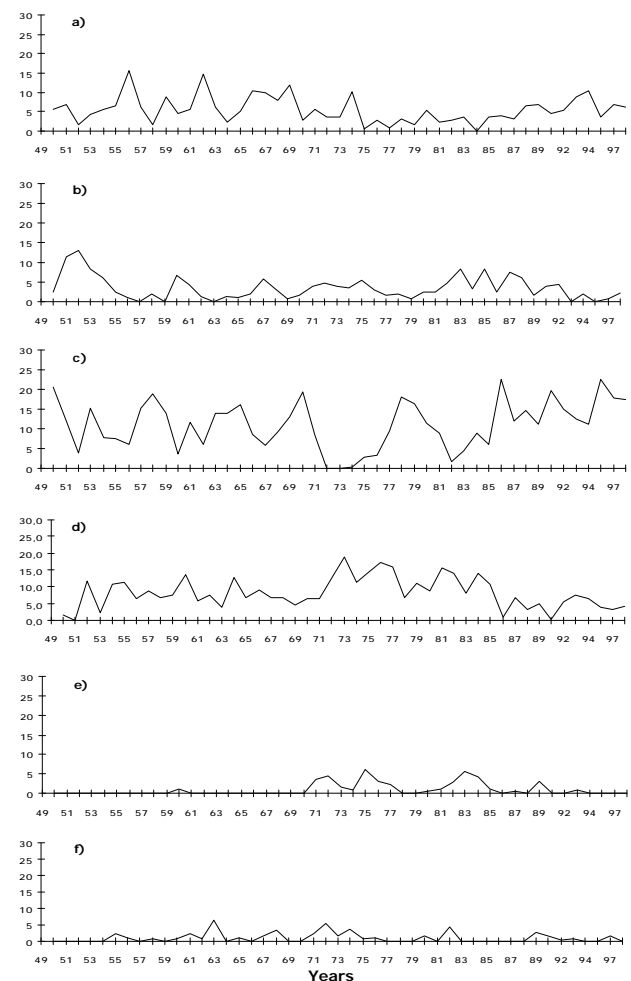


Figure 16. Five-month (November–March) winter mean time series (1949–1998) of frequency of occurrence for (a) Okhotsk–Aleutian, (b) Aleutian–Zonal, (c) Cyclones Over the North Pacific, (d) Northwest, (e) Okhotsk–Hawaii, and (f) Southern-Zonal synoptic situations over the North Pacific.

Figure 17 shows the time series (1949–1998) of sum frequency of occurrence (days/month) for CN and NW situations in (a) winter (including December of a previous year) and in (b) summer (May–September mean time series were used). Strong and medium El Niño events in winter are also marked. Minimums in the chart for (a) winter and maximums in the chart for (b) summer coincide with mostly El-Niño events, namely, the frequency of occurrence is low during the winter El Niño event in 1966 and reaches its local minimum during the winter El Niño events in 1973, 1983, 1987, and 1997, while it reaches local maxima in the summers of 1952, 1958, 1966, 1973, 1983, 1987, and 1992 following the winter El Niño events of the same years.

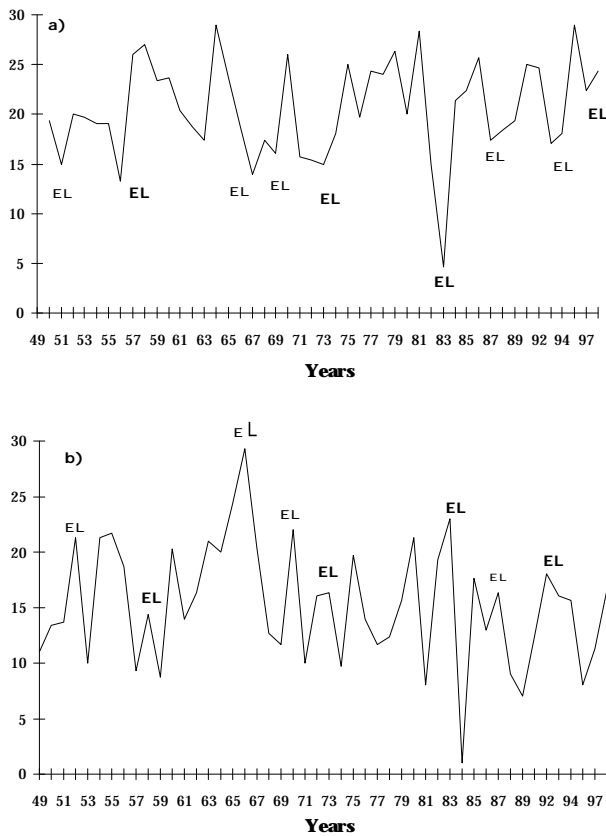


Figure 17. Time series (1949–1998) of sum frequency of occurrence for CN and NW synoptic situations over the North Pacific in (a) winter (for November–February mean values) and (b) summer (for May–September mean values). El Niño events are marked by EL symbols.

Thus, years of El Niño events dominating in winter are characterized by substantial anomalies in an annual cycle of the extratropical synoptic circulation patterns over the North Pacific. It seems that certain physical processes which control the accompanying ENSO effects in winter atmosphere over the mid-latitude Northwest Pacific are prominent in the cyclone track changes.

7. Conclusions

When analyzing conventional SST anomalies for the whole extratropical North Pacific (unfiltered monthly mean SST anomalies including anomalies of an annual cycle), the power spectrum has a maximum at the ENSO scale and a lagged correlation with SOI dominates, with SST being 1.5–2 years behind or 1 year ahead of the Niño3 Index. When analyzing interannual winter SST anomalies for the whole extratropical North Pacific (low-pass filtered wintertime monthly mean SST anomalies), an unlagged correlation with ENSO dominates and both ENSO and decadal scale variations are revealed.

In both cases the first CEOFs have maximums in the eastern and central Pacific while the second CEOFs are located in the Northwest Pacific. However, for the interannual winter SST anomalies the spatial core of the second mode is shifted to the north and confined in the transition area between the Oyashio and Kuroshio Currents where the most intensive ocean–atmosphere interaction takes place in winter. Presence of both decadal and ENSO variations in the SST anomalies as well as its unlagged/lagged significant correlation implies possible feedback between low-frequency variations of the two mentioned time scales in the mid-latitude Pacific and particularly in the Northwest Pacific also outlined by Sekine (1998).

The significant local maximums of the ENSO scale in spectra of monthly mean air temperature are pronounced for most of the seasons and meteorological stations in the Northwest Pacific Margin. Nevertheless, air temperature and SOI are related, in a different way, in the southern (South Japan Sea coast and Korean Peninsula), mid (Okhotsk Sea coast and Kamchatka Peninsula) and northern (Bering Sea coast and Chukchy Peninsula) areas. The principal difference is associated with the asymmetry of seasonal temperature anomalies in an annual cycle. Air temperature over the southern Japan Sea is under greater influence to ENSO-

accompanying dynamic processes in the extratropical summer atmosphere, while air temperature over the northern Japan Sea, Okhotsk Sea and Kamchatka Peninsula is mostly subjected to the impact of the ENSO accompanying processes in the winter atmosphere.

According to air temperature and SST analyses, one can suggest that ENSO and decadal scale variations in the North Pacific are connected via both annual–biennial oscillations of the Asian monsoon system and ocean–atmosphere interaction in the western mid-latitude (subarctic/subtropic) and central subtropic Pacific.

ENSO-accompanying processes in the Northwest Pacific increase frequency of occurrence of certain synoptic circulation patterns over the North Pacific associated mainly with cyclone track changes in the western margin. The ENSO signal with the lag of about half a year is associated with the Northwest Pacific ocean memory in a seasonal cycle. The ENSO signal with the lag of about one year is probably conditioned by both oceanic SST anomalies propagating from the tropic–equatorial Pacific to the extratropic areas and by the atmosphere circulation response to these anomalies.

References

- Alexander, M.A. 1992a. Midlatitude atmosphere–ocean interaction during El Niño. Part I: The North Pacific Ocean. *J. Climate*, 5, 944–958.
- Alexander, M.A. 1992b. Midlatitude atmosphere–ocean interaction during El Niño. Part II: The Northern Hemisphere Atmosphere. *J. Climate*, 5, 959–972.
- Barnston, A.G. and Livezey, R.E. 1987. Classification, seasonality and persistence of low-frequency atmospheric circulation patterns. *Mon. Wea. Rev.*, 115, 1083–1125.
- Bjerknes, J. 1969. Atmospheric teleconnections from the equatorial Pacific. *Mon. Wea. Rev.*, 97, 163–172.
- Blackmon, M.L., Wallace, J.M., Lau, N.-C. and Mullen, S.L. 1977. An observational study of the Northern Hemisphere wintertime circulation. *J. Atmos. Sci.*, 34, 1040–1053.
- Branstator, G.W. 1995. Organization of stormtrack anomalies by recurring low frequency circulation anomalies. *J. Atmos. Sci.*, 52, 207–226.
- Brillinger, D.R. 1975. *Time Series Data Analysis and Theory*. Holt, Rinehart and Winston, 500 pp.
- Chan, J.L. 1985. Tropical cyclone activity in west Pacific in relation to the El Niño/Southern Oscillation phenomenon. *Mon. Wea. Rev.*, 113, 599–606.
- Chen, T.C. and Weng, S.P. 1998. Interannual variation in the tropical cyclone formation over the western north Pacific. *Mon. Wea. Rev.*, 126, 1080–1090.
- Enting, I.G. and Robbins, F.J. 1989. Asymmetric filters for analyzing time series of atmospheric constituent data. *Tellus*, 41A, 109–114.
- Geisler, J.E., Backmon, M.L., Bates, G.T. and Munoz, S. 1985. Sensitivity of January climate response to the magnitude and position of equatorial Pacific sea surface temperature anomalies. *J. Atmos. Sci.*, 42, 1037–1049.
- Hanawa, K. 1995. Southward penetration of the Oyashio water system and the wintertime condition of midlatitude westerlies over the North Pacific. *Bull. Hokkaido Natl. Fish. Res. Inst.*, 59, 103–115.
- Hirst, A.C. 1986. Unstable and damped equatorial modes in simple coupled ocean–atmosphere models. *J. Atmos. Sci.* 43, 606–630.
- Horel, J.D. and Wallace, J.M. 1981. Planetary-scale atmospheric phenomena associated with the Southern Oscillation. *Mon. Wea. Rev.*, 109, 813–829.
- Horel, J.D. 1984. Complex principal component analysis: theory and examples. *J. Clim. Appl. Meteorol.*, 23, 1660–1673.
- Hou, A.Y. 1993. The influence of tropical heating displacements on the extratropical climate. *J. Atmos. Sci.*, 50, 3553–3570.
- Johnson, M.A. and O’Brien, J.J. 1990a. The role of coastal Kelvin waves on the northeast Pacific Ocean. *J. Marine Systems*, 1, 29–38.
- Johnson, M.A. and O’Brien, J.J. 1990b. The Northeast Pacific Ocean response to the 1982–1983 El Niño. *J. Geophys. Res.*, 95(C5), 7155–7166.
- Lau, K.M. and Boyle, J.S. 1987. Tropical and extratropical forcing of the large-scale circulation: a diagnostic study. *Mon. Wea. Rev.*, 11, 400–428.
- Lau, N.-C. and Nath, M.J. 1990. A general circulation model study of the atmospheric response to extratropical sea surface temperature anomalies observed in 1950–79. *J. Climate*, 3, 965–989.
- Learning to Predict Climate Variations Associated with El Niño and Southern Oscillation. Accomplishments and Legacies of the TOGA Program. 1996. National Academy Press. Washington, p. 235.
- Michaelson, J. 1982. A statistical study of large-scale, long-period variability in North Pacific sea surface temperature anomalies. *J. Phys. Oceanogr.*, 12, 694–703.
- Minster, J.-F. and Gennero, M.-C. 1995. High-frequency variability of western boundary currents using ERS 1 three-day repeat altimeter data. *J. Geophys. Res.*, 100(C11), 22,603–22,612.
- Mizuno, K. and White, W.B. 1983. Annual and interannual variability in the Kuroshio current system. *J. Phys. Oceanogr.*, 13, 1847–1867.
- Molteni, F., Ferranti, L., Palmer, T.N. and Viterbo, P. 1993. A dynamical interpretation of the global response to equatorial Pacific sea surface temperature anomalies. *J. Climate*, 6, 777–795.
- Nakamura, H., Lin, G. and Yamagata, T. 1997. Decadal climate variability in the North Pacific during the recent decades. *Bull. Amer. Meteorol. Soc.*, 78(10), 2215–2225.
- Oort, A.H. and Yienger, J.J. 1996. Observed interannual variability in the Hadley circulation and its connection to ENSO. *J. Climate*, 9, 2751–2767.
- Palmer, T.N. 1993. A nonlinear dynamical perspective on climate change. *Weather*, 48, 314–326.
- Philander, S.G.H., Yamagata, T. and Pacanowski, R.C. 1984. Unstable air–sea interactions in the tropics. *J. Atmos. Sci.*, 41, 604–613.

- Plotnikov, V.V. 1997. Space-time relations between ice conditions in the Far Eastern Seas. *Meteorol. Gidrol.*, 3, 77–85 (Rus.).
- Polyakova, A.M. 1992. Method of Super Long Term Forecast of Ice Covering of the Okhotsk Sea. *The Seventh International Symposium on Okhotsk Sea and Sea Ice. Cold Research Association, Mombetsu, Japan*, 375–376.
- Polyakova, A.M. 1997. The types of atmospheric circulation over the North Pacific and climate variations in the North Pacific. *Pacific Oceanological Institute. Proceedings of Annual Session, 1994. Dalnauka, Vladivostok, Russia*, 98–105 (Rus.).
- Schucla, J. and Paolino, D.A. 1983. The Southern oscillation and long-range forecasting of the summer monsoon rainfall over India. *Mon. Wea. Rev.*, 111, 1830–1837.
- Sekine, Y. 1996. Anomalous Oyashio intrusion and its teleconnection with Subarctic North Pacific circulation, sea ice of the Okhotsk Sea and air temperature of the northern Asian continent. *Proceedings of PICES Workshop on the Okhotsk Sea and Adjacent Areas., Vladivostok, June 19–24, 1995. Canada, 1996*, 177–187.
- Sekine, Y. and Yamada, F. 1996. Atmosphere and ocean global teleconnection around the Okhotsk Sea. *The 11th International Symposium on Okhotsk Sea and Sea Ice, 25–28 February 1996, Mombetsu, Hokkaido, Japan. Abstracts*, 148–150.
- Sekine, Y. 1998. On the teleconnection processes around the North Pacific with reference to the decadal variations in atmosphere and ocean. *Seventh Annual PICES Meeting, Abstracts, October 14–25, 1998. Fairbanks*, p. 39.
- Simmons, A.J., Wallace, J.M. and Branstator, G.W. 1983. Barotropic wave propagation and instability, and atmospheric teleconnection patterns. *J. Atmos. Sci.*, 40, 1363–1392.
- Tanaka, M. 1982. Interannual fluctuations of the tropical winter monsoon circulation and its relationship to the Walker circulation. *Tropical Ocean – Atmos. Newslett.*, 12, 4–5.
- Trenberth, K.E. and Paolino, D.A. 1981. Characteristic patterns of variability of sea level pressure in the Northern Hemisphere. *Mon. Wea. Rev.*, 109, 1169–1189.
- Trenberth, K.E. 1995. El Niño / Southern Oscillation. *in Climate Change: Developing Southern Hemisphere Perspectives*, T.W. Giambelluca and A. Henderson-Sellers (eds.), Wiley, New York, chap. 6.
- Trousenkov, S.T. 1991. Identifying waves in climate signal processing. *Proc. Intern. AMSE Conf. "Signals & Systems". Warsaw, Poland, July 15–17, 1991, Vol. 5*, 145–153.
- Wallace, J.M. and Gutzler, D.S. 1981. Teleconnections in the geopotential height field during the Northern Hemisphere winter. *Mon. Weather Rev.*, 109, 784–812.
- Walker, G.T. 1924. Correlation in seasonal variations of weather IX: A further study of world weather. *Mem. Indian Meteor. Dept.*, 24 (4), 275–332.
- Watanabe, T., Hanava, K. and Toba, Y. 1986. Analysis of year-to-year variation of water temperature along the coast of Japan Sea. *Prog. Oceanogr.*, 17, 337–357.
- Webster, P.J. and Yang, S. 1992. Monsoon and ENSO: selectively interactive systems. *Quart. J. Roy. Meteorol. Soc.*, 118, 877–926.
- Webster, P.J., Dixit, S. and Palmer, T.N. 1997. Intraseasonal variability of the Monsoon system and its relationship to monsoon predictability on interannual timescales: the concept of nudged chaos. *Joint Assemblies of IAMAS and IAPSO*, JMP1-31.
- Wu, M.C. and Hastenrath, S. 1986. On the interannual variability of the Indian monsoon and the Southern oscillation. *Arch. Meteor. Geophys. Biocl.*, B39, 239–261.
- Wyrтки, K. 1975. El Niño – The dynamic response of the equatorial Pacific Ocean to atmospheric forcing. *J. Phys. Oceanogr.*, 5, 572–584.
- Yang, S. and Webster, P.J. 1990. The effect of summer tropical heating on the location and intensity of the extratropical westerly jet streams. *J. Geophys. Res.*, 95(D11), 18,705–18,721.
- Zhang, Y. and Wallace, J.M. 1996. Is climate variability over the North Pacific a linear response to ENSO? *J. Climate*, 9, 1468–1478.